inverse problems and machine learning at the service of space science

michele piana

dipartimento di matematica
università di genova

CNR - SPIN, genova

SIMAI 2018, roma, july 2 2018

space weather

space weather results from a sophisticated interplay of different scientific disciplines with the aim of **understanding** and **predicting** the connection between the solar activity and the physical conditions throughout the interplanetary space down into the planets' atmosphere

space weather

space weather results from a sophisticated interplay of different scientific disciplines with the aim of **understanding** and **predicting** the connection between the solar activity and the physical conditions throughout the interplanetary space down into the planets' atmosphere

space weather is challenging for **physics** because the dynamics of the solar atmosphere is poorly known and its comprehension is crucial for unveiling what happens in more remote and more mysterious astrophysical objects

space weather

space weather results from a sophisticated interplay of different scientific disciplines with the aim of **understanding** and **predicting** the connection between the solar activity and the physical conditions throughout the interplanetary space down into the planets' atmosphere

space weather is challenging for **physics** because the dynamics of the solar atmosphere is poorly known and its comprehension is crucial for unveiling what happens in more remote and more mysterious astrophysical objects

space weather is challenging for **mathematics** because up-to-date models involve difficult PDEs and because the remoteness of the information source implies ill-posedness in the sense of hadamard

space weather

space weather results from a sophisticated interplay of different scientific disciplines with the aim of **understanding** and **predicting** the connection between the solar activity and the physical conditions throughout the interplanetary space down into the planets' atmosphere

space weather is challenging for **physics** because the dynamics of the solar atmosphere is poorly known and its comprehension is crucial for unveiling what happens in more remote and more mysterious astrophysical objects

space weather is challenging for **mathematics** because up-to-date models involve difficult PDEs and because the remoteness of the information source implies ill-posedness in the sense of hadamard

space weather is timely because the quantity and quality of **data** we will have at disposal in the next decade will be overwhelming

space weather at earth

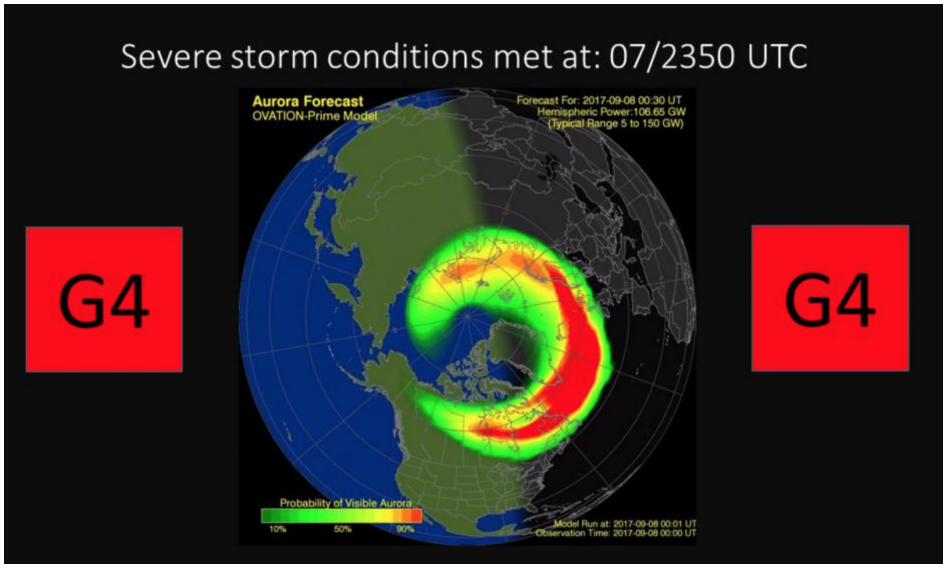

space weather at earth

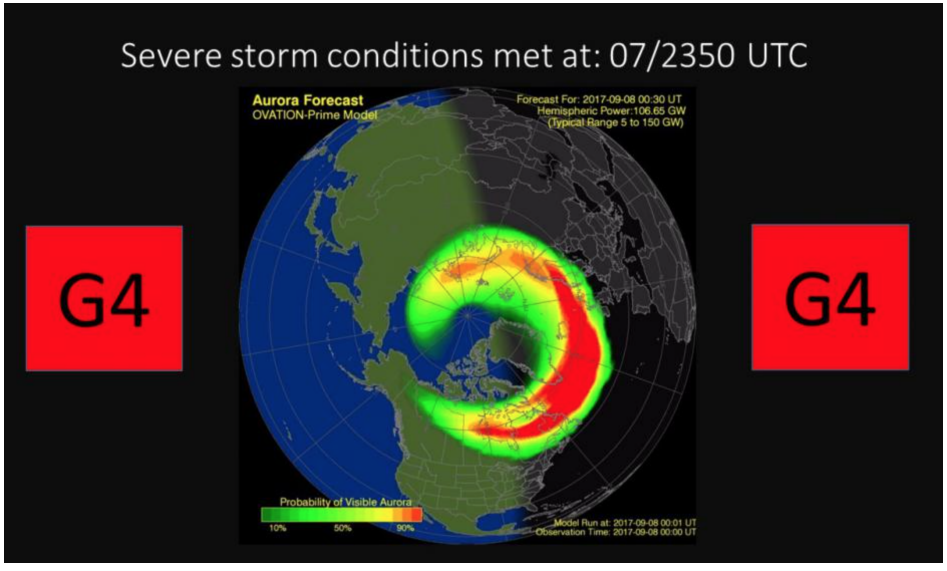

space weather at earth

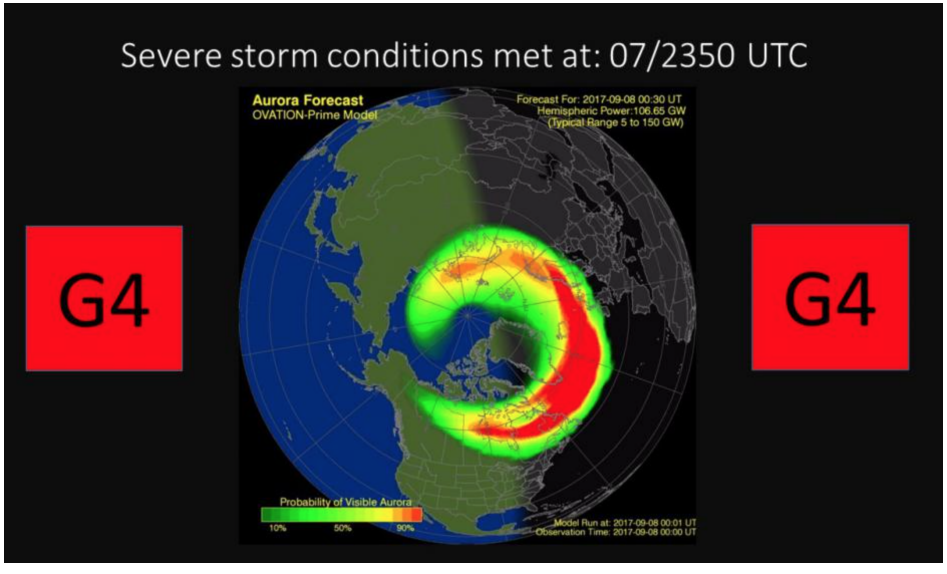

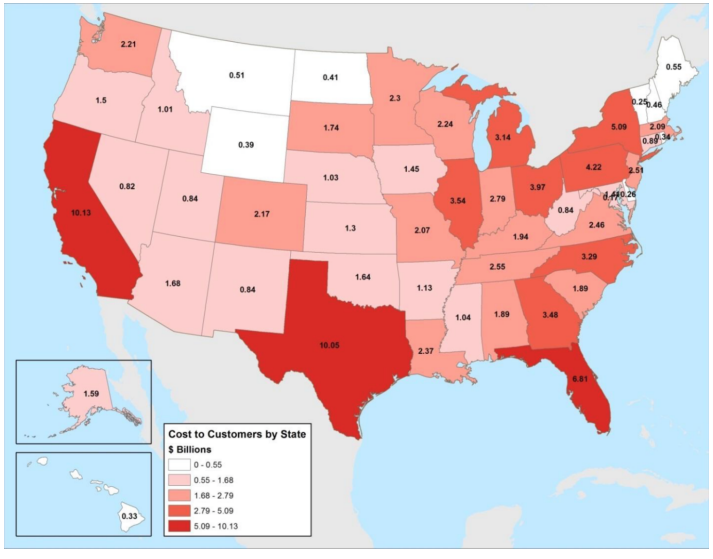

space weather at earth

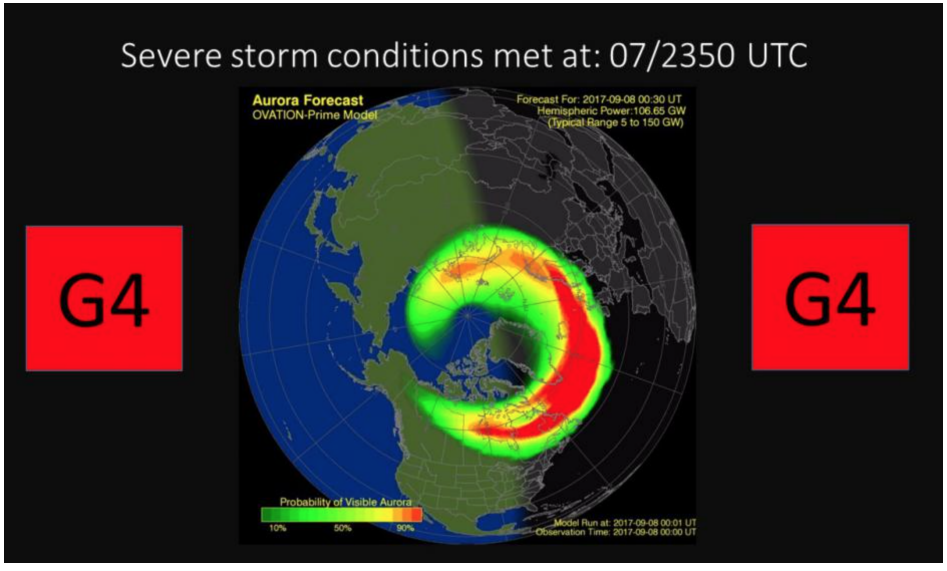

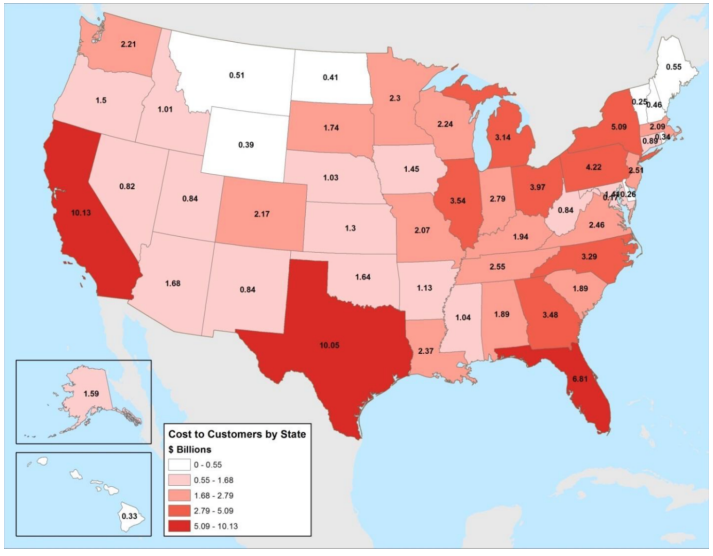

solar flares

- extend over $10,000$ km
- release more than 10^{32} erg in less than 100 s
- accelerate billions of tons of material to more than 10^6 km/h
- emit electromagnetic radiation at all wavelengths
- trigger the whole space weather connection

the flare paradox

- inductance: 10^{-6} henry
- voltage: 220 volt
- light-up time (predicted): 10^{-9} s
- light-up time (observed): instantaneous

the flare paradox

- inductance: 10^{-6} henry
- voltage: 220 volt
- light-up time (predicted): 10^{-9} s
- light-up time (observed): instantaneous

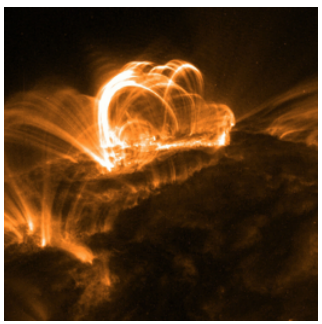

- inductance: 10 henry
- voltage: 10^{6} volt
- light-up time (predicted): 3×10^{5} years
- light-up time (observed): no more than some minutes

industry 4.0 in space

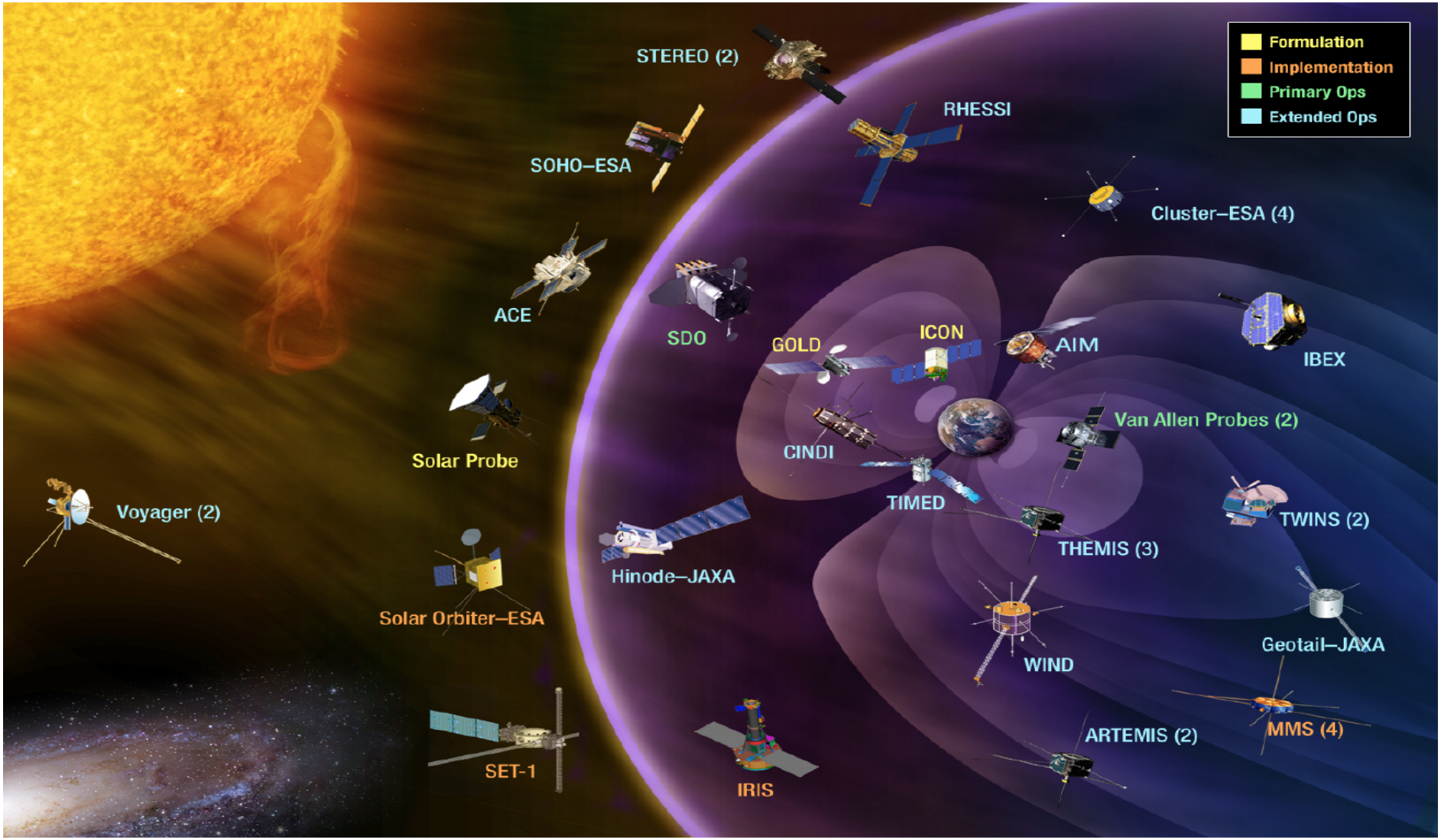

outline of the talk

flares and math:

- artificial intelligence and flare prediction:
  - pattern recognition extracts features from the experimental data
  - machine learning utilizes the extracted features for binary prediction
  - regularization networks compute the feature impact to forecast
  - multi-task learning allows the prediction of flare-related parameters

outline of the talk

flares and math:

- artificial intelligence and flare prediction:
  - pattern recognition extracts features from the experimental data
  - machine learning utilizes the extracted features for binary prediction
  - regularization networks compute the feature impact to forecast
  - multi-task learning allows the prediction of flare-related parameters
- inverse problems and flare morphology reconstruction
  - space telescopes provide indirect signatures of the flaring topography
  - inverse problems methods realize the transition from remote sensing to physically meaningful images

outline of the talk

flares and math:

- artificial intelligence and flare prediction:
  - pattern recognition extracts features from the experimental data
  - machine learning utilizes the extracted features for binary prediction
  - regularization networks compute the feature impact to forecast
  - multi-task learning allows the prediction of flare-related parameters
- inverse problems and flare morphology reconstruction
  - space telescopes provide indirect signatures of the flaring topography
  - inverse problems methods realize the transition from remote sensing to physically meaningful images
- inverse problems and MHD-based flare modeling
  - MHD combines maxwell's equations and navier-stokes equation in extreme thermodynamical conditions
  - MHD-based models of solar flares can be calibrated by using optimization of inverse problems

flare prediction

AR 12673

data: helioseismic and magnetic imager in the solar dynamics observatory (SDO/HMI)

- flares originate from active regions (ARs)
- just a few ARs originate flare
- SDO/HMI provides vector magnetograms every 12 minutes, with clearly visible ARs
- on august 30 2017 AR 12673 became visible on a full disk HMI magnetogram. would it be possible to predict the flare occurrence from it?

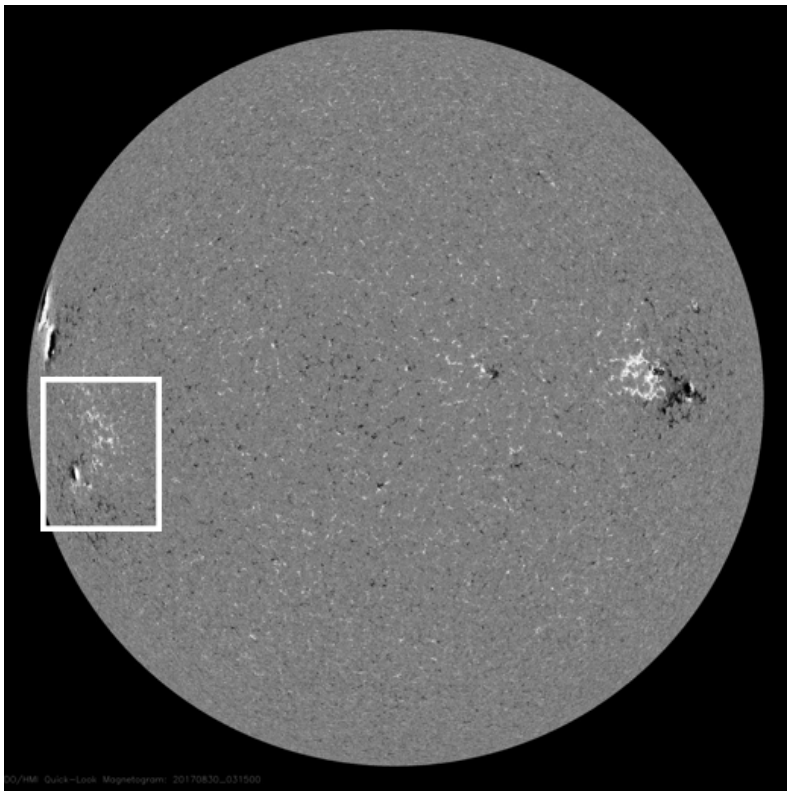

supervised machine learning

ingredients:

- a historical data set (e.g.: a set of magnetograms in the HMI archive)
- a feature set extracted by pattern recognition from each element of the historical data set (e.g.: image features extracted from ARs in HMI magnetograms)
- a set of labels, each one associated to a feature set and encoding the outcome information (e.g.: a label testifying the flare occurrence and intensity)
- a machine learning method

supervised machine learning

ingredients:

- a historical data set (e.g.: a set of magnetograms in the HMI archive)
- a feature set extracted by pattern recognition from each element of the historical data set (e.g.: image features extracted from ARs in HMI magnetograms)
- a set of labels, each one associated to a feature set and encoding the outcome information (e.g.: a label testifying the flare occurrence and intensity)
- a machine learning method

the supervised scheme:

1. the machine learning method is trained by means of the historical (training) set and the corresponding set of labels
2. a new data arrives (e.g.: a new magnetogram)
    1. the pattern recognition method extracts the features from it
    2. the machine learning method predicts the outcome corresponding to the new feature set (e.g.: will the flare occur within a given time range?)

training set and labels

- historical set: full-disk HMI magnetograms in the time range 2012-2016 with 6 hour cadence (i.e., $4 \times 365 \times 5 = 7300$ images)
- 20 features extracted from each AR by means of segmentation and other image processing methods (i.e., more than 7300 feature vector of dimension 20)
- labels: binary + a number indicating the class associated to the flare intensity (C, M, X)

hybrid LASSO (benvenuto, p, campi and massone, *ApJ*, 2018)

for each flare class

phase 1: training (LASSO)

$$X \in \mathbb{R}^{N \times F} \quad y \in \mathbb{R}^{N \times 1} \quad \beta \in \mathbb{R}^{F \times 1}$$

$$\hat{\beta} = \arg\min_{\beta}(\|y - X\beta\|_2^2 + \lambda\|\beta\|_1)$$

hybrid LASSO (benvenuto, p, campi and massone, *ApJ*, 2018)

for each flare class

phase 1: training (LASSO)

$$X \in \mathbb{R}^{N \times F} \quad y \in \mathbb{R}^{N \times 1} \quad \beta \in \mathbb{R}^{F \times 1}$$

$$\hat{\beta} = \arg\min_{\beta}(\|y - X\beta\|_2^2 + \lambda\|\beta\|_1)$$

phase 2: prediction (fuzzy clustering)

$$\hat{y} = X\hat{\beta}$$

$$U \in \mathbb{R}^{2 \times N} \quad u_{jk} \in [01,] \quad z = \{z_j | z_j \in \mathbb{R}\ ,\ j = 1,2\} \quad d_{jk} = d_{jk}(z, \hat{y})$$

$$(\hat{z}, \hat{U}) = \arg\min_{(z,U)} \sum_{k=1}^{N} \sum_{j=1}^{2} (u_{jk})^m d_{jk}^2$$

hybrid LASSO (benvenuto, p, campi and massone, *ApJ*, 2018)

for each flare class

phase 1: training (LASSO)

$$X \in \mathbb{R}^{N \times F} \quad y \in \mathbb{R}^{N \times 1} \quad \beta \in \mathbb{R}^{F \times 1}$$

$$\hat{\beta} = \arg\min_{\beta}(\|y - X\beta\|_2^2 + \lambda\|\beta\|_1)$$

phase 2: prediction (fuzzy clustering)

$$\hat{y} = X\hat{\beta}$$

$$U \in \mathbb{R}^{2 \times N} \quad u_{jk} \in [01,] \quad z = \{z_j | z_j \in \mathbb{R}\ ,\ j = 1,2\} \quad d_{jk} = d_{jk}(z, \hat{y})$$

$$(\hat{z}, \hat{U}) = \arg\min_{(z,U)} \sum_{k=1}^{N} \sum_{j=1}^{2} (u_{jk})^m d_{jk}^2$$

when x_{new} arrives, $x_{new}^t \hat{\beta}$ is compared to $\hat{z}_1$ and $\hat{z}_2$ in order to decide the cluster to which it belongs

the september 2017 super-storm

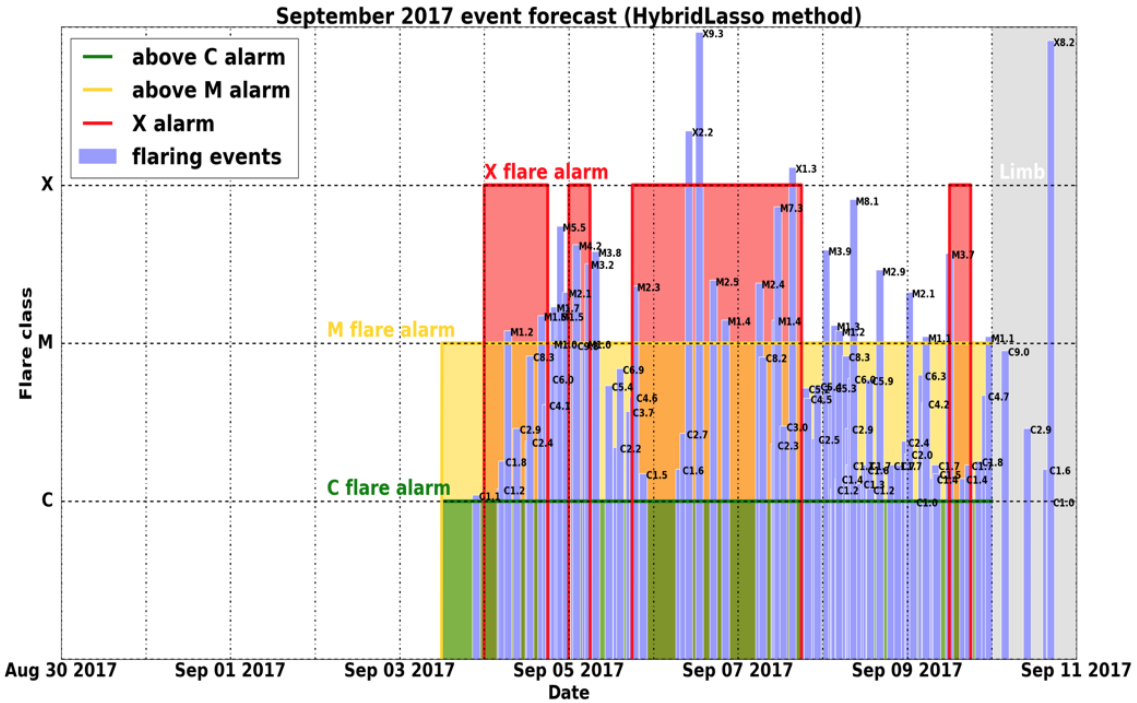

the september 2017 super-storm

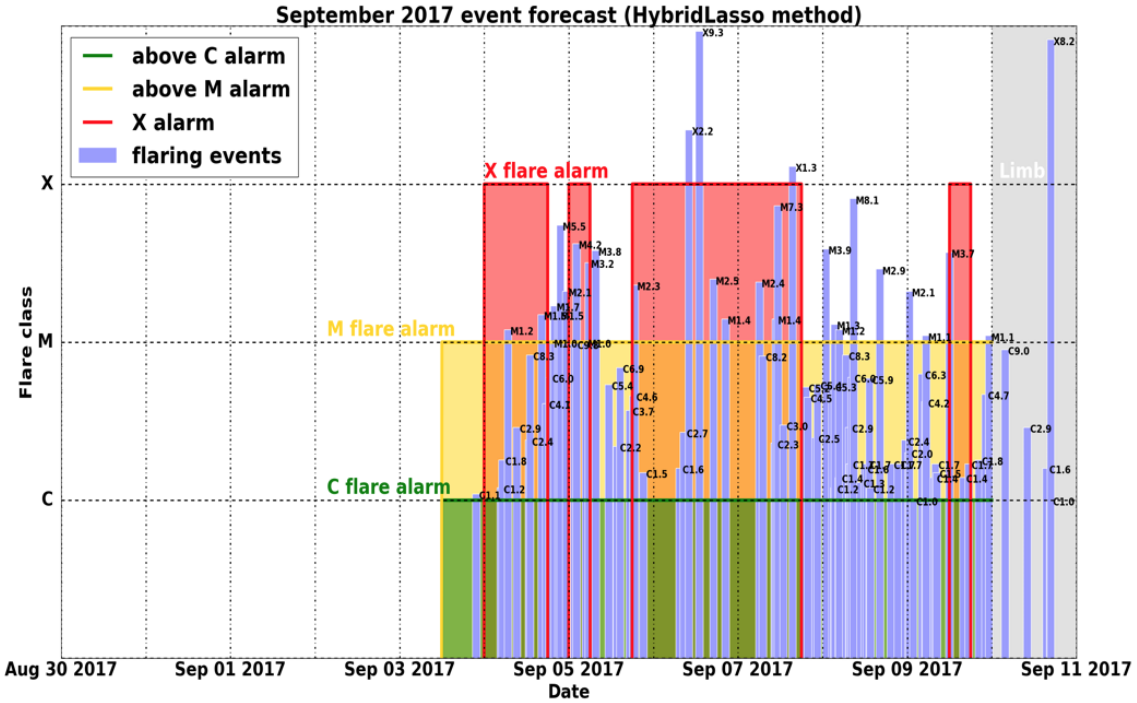

FLARECAST

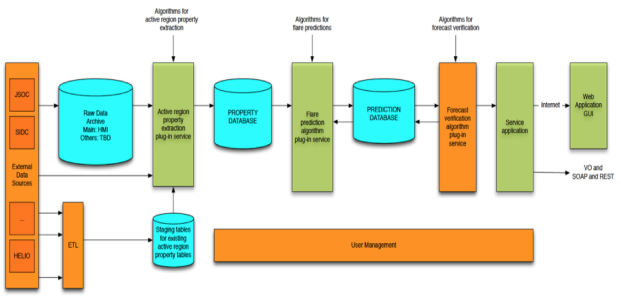

flare morphology

the extreme ultraviolet sun

data: atmospheric imaging assembly in the solar dynamics observatory (SDO/AIA)

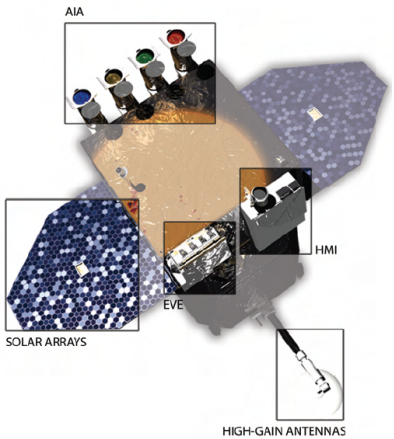

good news: SDO/AIA provides

- 7 full disk 4096×4096 pixel resolution images every 12 second
- in 7 different wavelength (extreme ultraviolet, EUV)
- with the best spatial resolution ever

the extreme ultraviolet sun

data: atmospheric imaging assembly in the solar dynamics observatory (SDO/AIA)

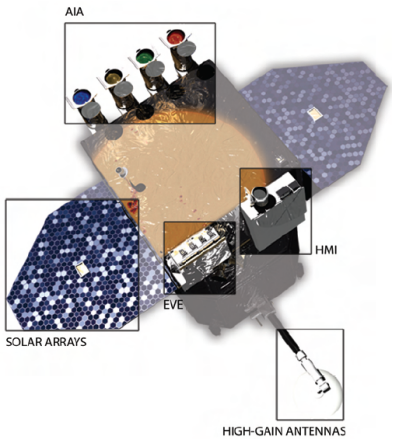

good news: SDO/AIA provides

- 7 full disk 4096×4096 pixel resolution images every 12 second
- in 7 different wavelength (extreme ultraviolet, EUV)
- with the best spatial resolution ever

bad news: more than 10^5 images per year are affected by

- diffraction
- saturation
- blooming

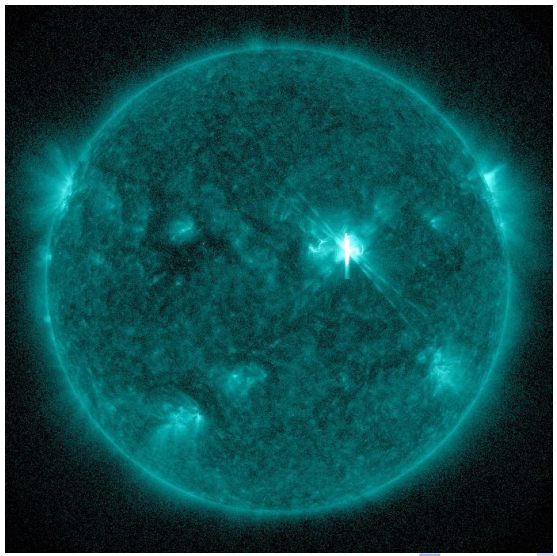

the extreme ultraviolet sun

data: atmospheric imaging assembly in the solar dynamics observatory (SDO/AIA)

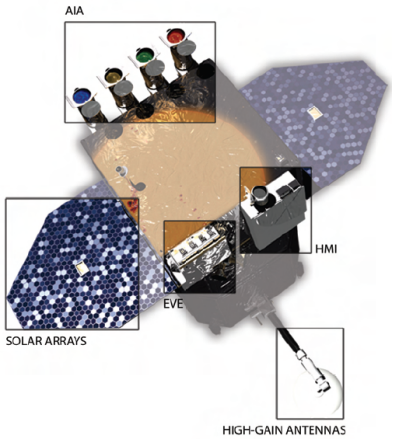

good news: SDO/AIA provides with

- 7 full disk 4096×4096 pixel resolution images every 12 second
- in 7 different wavelength (extreme ultraviolet, EUV)
- with the best spatial resolution ever

bad news: more than 10^5 images per year are affected by

- diffraction
- saturation
- blooming

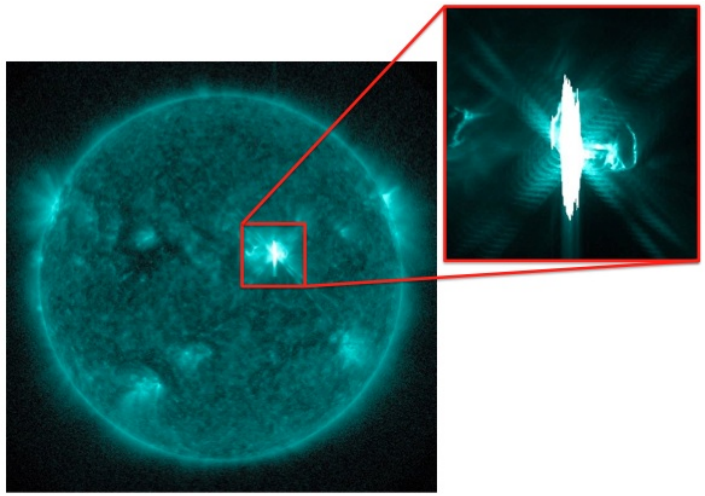

saturation, blooming, diffraction

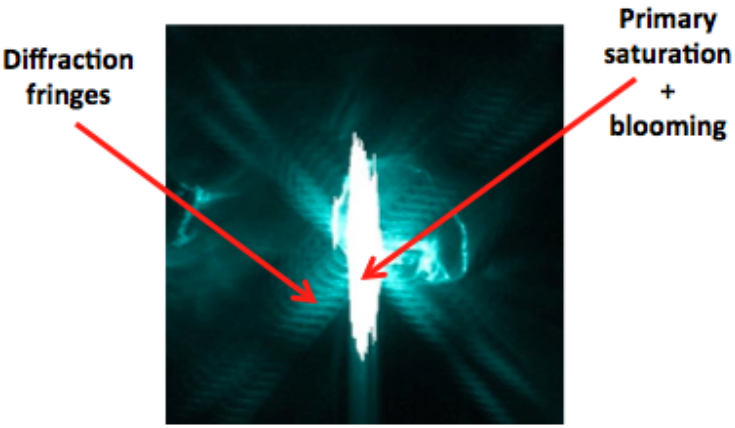

- **primary saturation**: some pixels reach the full well capacity, i.e. they store the maximum number possible of photon-induced electrons
- **blooming**: at saturation, pixels lose their ability to accommodate additional charge, which spreads into neighboring pixels, causing second-order saturation. such spread of charge typically shows up as a bright artifact along a privileged axis in the image
- **diffraction**: telescope hardware generates diffraction fringes proportional to the incoming radiation intensity

all information on the radiation flux lost due to primary saturation is actually present in the diffraction pattern and therefore the signal in the primary saturation region can be restored by solving an inverse diffraction problem

point spread function (PSF)

image formation process:

$$A : L^2(\mathbb{R}^2) \to L^2(\mathbb{R}^2) \quad (Af)(x,y) = \int_{\mathbb{R}^2} K(x-x';y-y')f(x',y')dx'dy'$$

$$I(x,y) = (Af)(x,y) \quad (x,y) \in \mathbb{R}^2$$

point spread function (PSF)

image formation process:

$$A : L^2(\mathbb{R}^2) \to L^2(\mathbb{R}^2) \quad (Af)(x,y) = \int_{\mathbb{R}^2} K(x-x';y-y')f(x',y')dx'dy'$$

$$I(x,y) = (Af)(x,y) \quad (x,y) \in \mathbb{R}^2$$

finite-dimensional setting:

$$I = Af$$

- f is a vector of size N representing the incoming radiation field
- I is a vector of size N representing the signal recorded from the CCD
- A is a $N \times N$ circulant matrix associated to the PSF

point spread function (PSF)

image formation process:

$$A : L^2(\mathbb{R}^2) \to L^2(\mathbb{R}^2) \quad (Af)(x,y) = \int_{\mathbb{R}^2} K(x-x';y-y')f(x',y')dx'dy'$$

$$I(x,y) = (Af)(x,y) \quad (x,y) \in \mathbb{R}^2$$

finite-dimensional setting:

$$I = Af$$

- f is a vector of size N representing the incoming radiation field
- I is a vector of size N representing the signal recorded from the CCD
- A is a $N \times N$ circulant matrix associated to the PSF

$A = A_D + A_C$ where

- A_D diffraction component $\Longrightarrow$
- A_C diffusion component

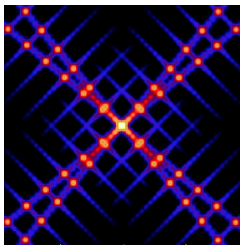

de-saturation problem

ingredients:

- $\mathcal{N}$ set of pixels (known)
- S_P set of pixels where **primary saturation** occurred (unknown)
- B set of pixels where **blooming** occurred (unknown)
- $S = S_P \cup B$ set of saturated pixels (known)
- F_P $(F_P \cap S = \emptyset)$ set of pixels corresponding to the diffraction fringes (unknown)
- f_P radiation field in S_P (unknown)
- f_S radiation field in S (unknown)
- BG total background (unknown)

the problem: reconstruction of an image I_{desat} where information in S_P and B are recovered and where diffraction fringes in F_P are removed

inverse diffraction: mathematical setup

$$F = \{i \notin S \ , \ (A_D \chi_S)_i \neq 0\} \qquad F \supset F_P \qquad I_F = \{I_i \ , \ i \in F\}$$

$$A_D^S : \mathbb{R}^{\sharp S} \to \mathbb{R}^{\sharp F}$$

$$I_F = A_D^S f_S + BG_F$$

note 1: to estimate the background BG_F, use interpolation of the non-saturated images just before and just after the saturated one

note 2: we are assuming that diffraction effects associated to pixels out of the primary saturation region are negligible

inverse diffraction: expectation maximization (EM)

$$I_F = A_D^S f_S + BG_F$$

inverse diffraction: expectation maximization (EM)

$$I_F = A_D^S f_S + BG_F$$

$$p(I_F|f_S) = \prod_{i=1}^{\sharp F} \frac{e^{-(A_D^S f_S + BG_F)_i}}{(I_F)_i!} (A_D^S f_S + BG_F)_i^{(I_F)_i}$$

inverse diffraction: expectation maximization (EM)

$$I_F = A_D^S f_S + BG_F$$

$$p(I_F|f_S) = \prod_{i=1}^{\sharp F} \frac{e^{-(A_D^S f_S + BG_F)_i}}{(I_F)_i!} (A_D^S f_S + BG_F)_i^{(I_F)_i}$$

$$\max_{f_S \geq 0} p(I_F|f_S)$$

inverse diffraction: expectation maximization (EM)

$$I_F = A_D^S f_S + BG_F$$

$$p(I_F|f_S) = \prod_{i=1}^{\sharp F} \frac{e^{-(A_D^S f_S + BG_F)_i}}{(I_F)_i!} (A_D^S f_S + BG_F)_i^{(I_F)_i}$$

$$\max_{f_S \geq 0} p(I_F|f_S)$$

theorem (KKT):

$$f_S = f_S (A_D^S)^T \left(\frac{I_F}{A_D^S f_S + BG_F} \right)$$

inverse diffraction: expectation maximization (EM)

$$I_F = A_D^S f_S + BG_F$$

$$p(I_F|f_S) = \prod_{i=1}^{\sharp F} \frac{e^{-(A_D^S f_S + BG_F)_i}}{(I_F)_i!} (A_D^S f_S + BG_F)_i^{(I_F)_i}$$

$$\max_{f_S \geq 0} p(I_F|f_S)$$

theorem (KKT):

$$f_S = f_S (A_D^S)^T \left(\frac{I_F}{A_D^S f_S + BG_F} \right)$$

algorithm (EM):

$$f_S^{(k+1)} = \frac{f_S^{(k)}}{A_D \mathbf{1}} (A_D^S)^T \left(\frac{I_F}{A_D^S f_S^{(k)} + BG_F} \right)$$

inverse diffraction: stopping rule

$$f_S^{(k+1)} = \frac{f_S^{(k)}}{A_D \mathbf{1}} (A_D^S)^T \left(\frac{I_F}{A_D^S f_S^{(k)} + B G_F} \right)$$

inverse diffraction: stopping rule

$$f_S^{(k+1)} = \frac{f_S^{(k)}}{A_D \mathbf{1}} (A_D^S)^T \left(\frac{I_F}{A_D^S f_S^{(k)} + B G_F} \right)$$

$$f_S^{(k)} \to 0 \quad \text{or} \quad \alpha^{(k)} := \frac{(A_D^S)^T \left(\frac{I_F}{A_D^S f_S^{(k)} + B G_F} \right)}{A_D^S \mathbf{1}} \to 1$$

inverse diffraction: stopping rule

$$f_S^{(k+1)} = \frac{f_S^{(k)}}{A_D \mathbf{1}} (A_D^S)^T \left(\frac{I_F}{A_D^S f_S^{(k)} + B G_F} \right)$$

$$f_S^{(k)} \to 0 \quad \text{or} \quad \alpha^{(k)} := \frac{(A_D^S)^T \left(\frac{I_F}{A_D^S f_S^{(k)} + B G_F} \right)}{A_D^S \mathbf{1}} \to 1$$

$$z^{(k)} := \| f_S^{(k)} (A_D^S)^T \left(\mathbf{1} - \frac{I_F}{A_D^S f_S^{(k)} + B G_F} \right) \|^2 \to 0$$

inverse diffraction: stopping rule

$$f_S^{(k+1)} = \frac{f_S^{(k)}}{A_D \mathbf{1}} (A_D^S)^T \left(\frac{I_F}{A_D^S f_S^{(k)} + B G_F} \right)$$

$$f_S^{(k)} \to 0 \quad \text{or} \quad \alpha^{(k)} := \frac{(A_D^S)^T \left(\frac{I_F}{A_D^S f_S^{(k)} + B G_F} \right)}{A_D^S \mathbf{1}} \to 1$$

$$z^{(k)} := \| f_S^{(k)} (A_D^S)^T \left(\mathbf{1} - \frac{I_F}{A_D^S f_S^{(k)} + B G_F} \right) \|^2 \to 0$$

theorem (torre, schwartz, benvenuto, massone and p, *inverse problems*, 2015): the rule $z^{(k)} = E(z^{(k)})$ is a regularization algorithm in both the classical and the asymptotical sense

segmentation

S is known and f_S has been determined as described $\Rightarrow$ the image is segmented in three regions:

primary saturation:

- S_P is the set of pixels where $A_C^S f_S$ is above the saturation threshold
- $f_P = \{(f_S)_i \ , \ i \in S_P\}$
- $I_P = \{(A_C^S f_S)_i \ , \ i \in S_P\}$

with A_C^S sub-matrix of A_C restricted to S

blooming:

- $B = S \setminus S_P$
- BG_B sub-matrix of BG restricted to B

diffraction fringes:

- $F_P = \{i \in \mathcal{N} \ , \ (A_D \chi_{S_P})_i \neq 0\}$
- $A_D^{S_P}$ sub-matrix of A_D s.t. $A_D^{S_P} : \mathbb{R}^{\sharp S_P} \rightarrow \mathbb{R}^{\sharp F_P}$
- $I_{F_P} = I_{\restriction F_P} - A_D^{S_P} f_P$

de-saturated image

the solution of the de-saturation problem is:

$$I_{\text{desat}} = \begin{cases} I_P & \text{in} \quad S_P \\ BG_B & \text{in} \quad B \\ I_{FP} & \text{in} \quad F_P \\ I & \text{otherwise} \end{cases}$$

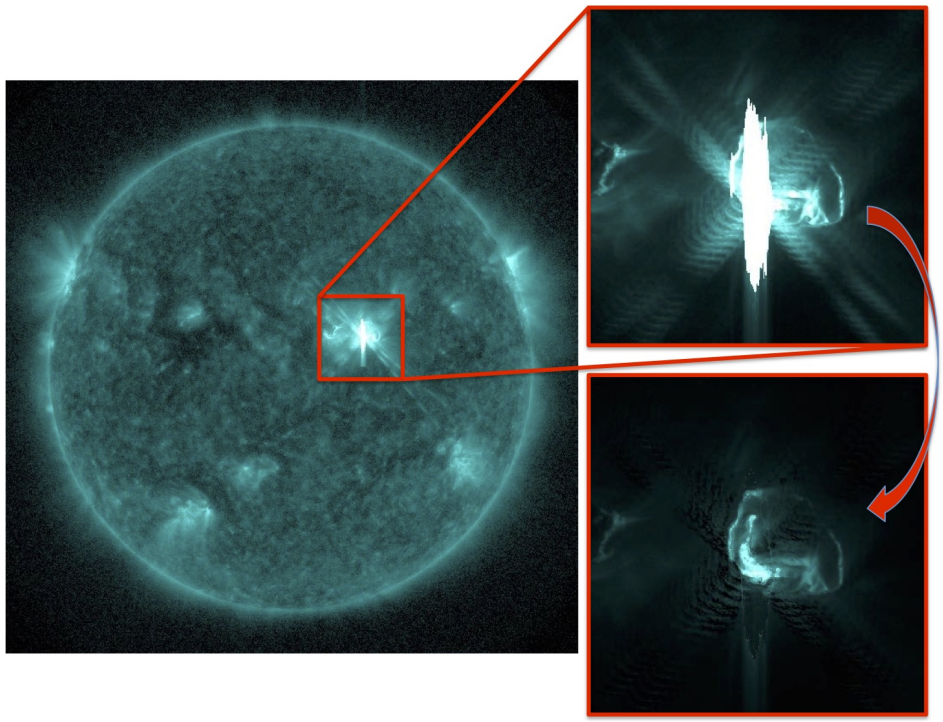

september 6, 2011 - 131 Å

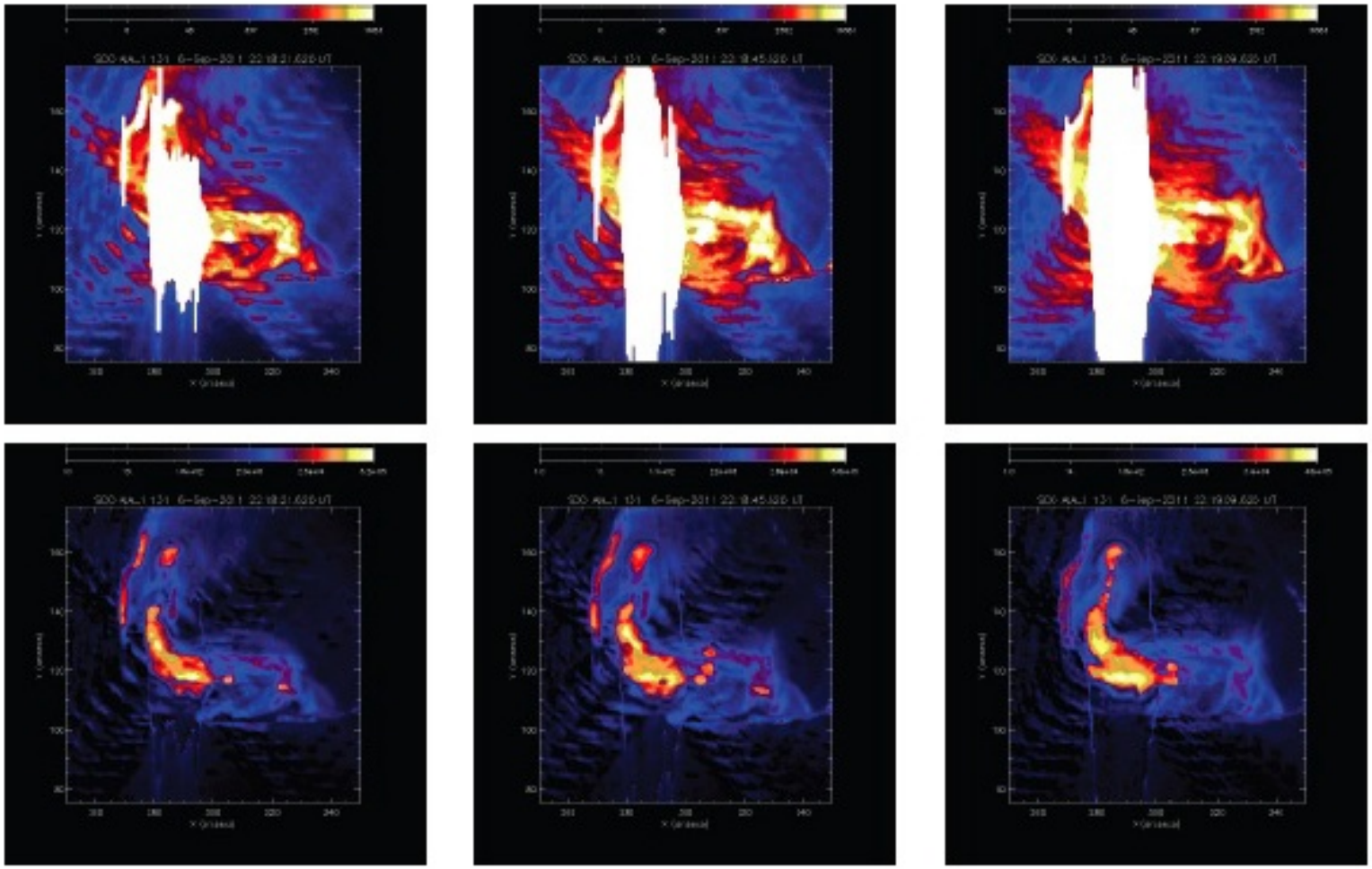

flare physics

physics interlude

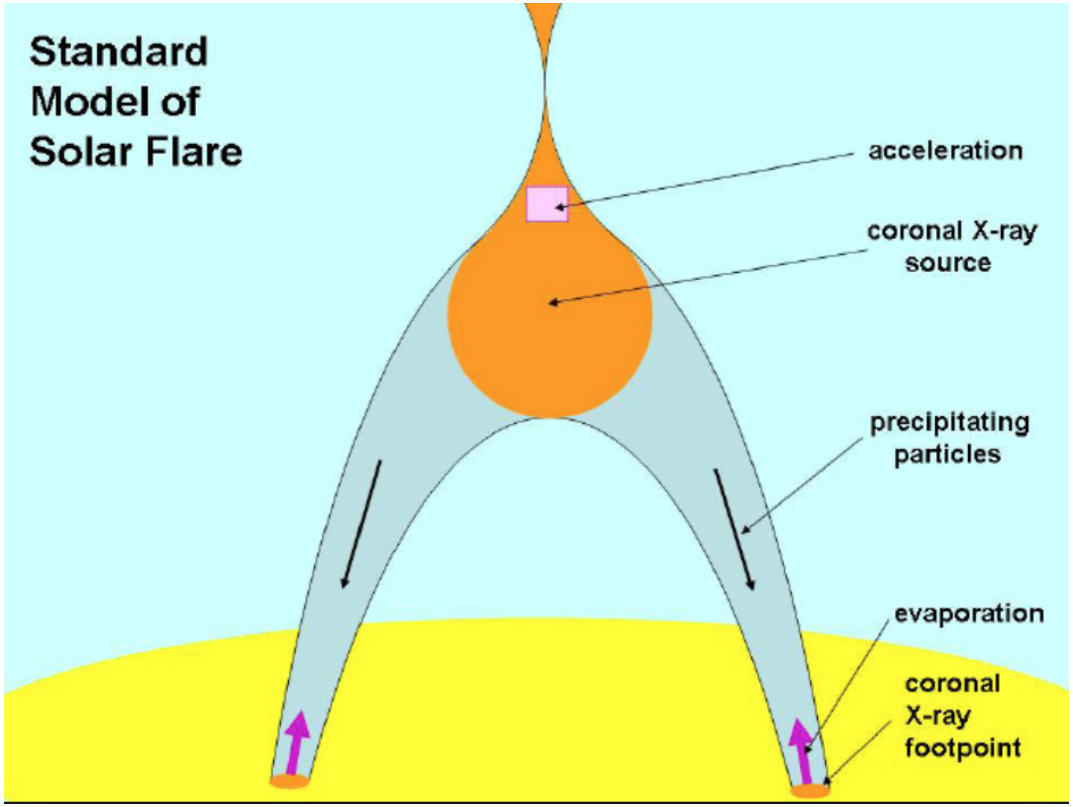

physics interlude

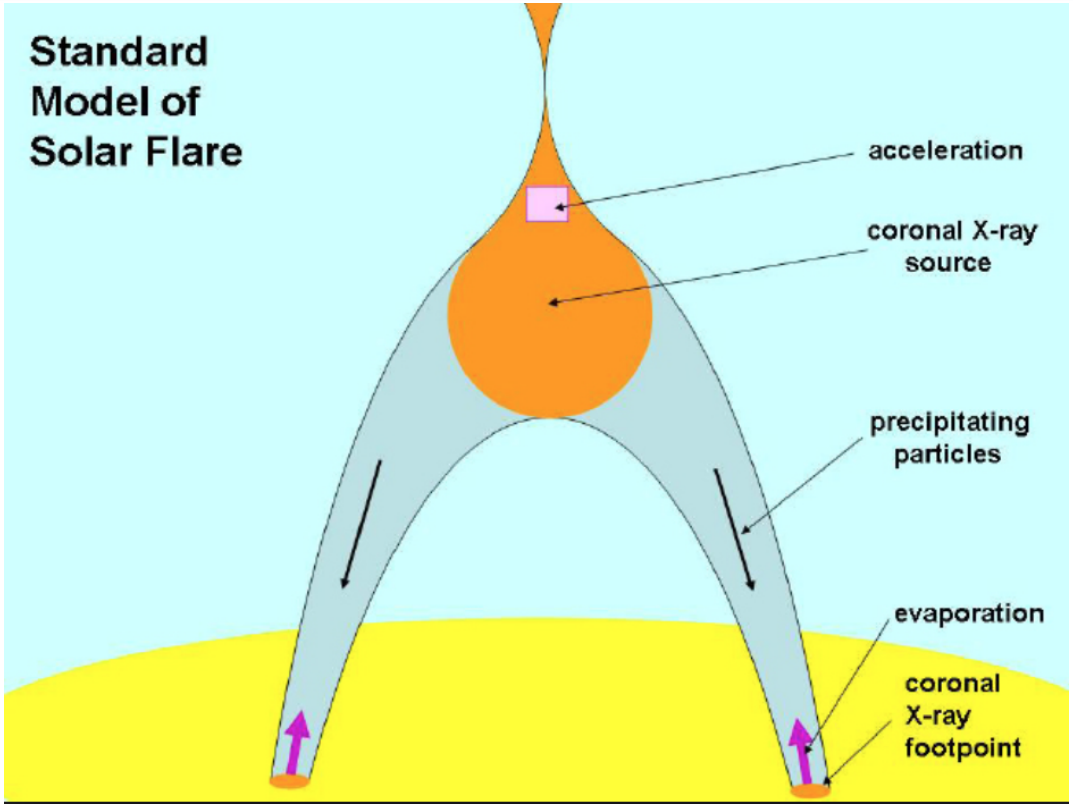

$$\frac{\partial F(E;s)}{\partial s} + \frac{\partial}{\partial E}\left(F(E,s)\frac{dE}{ds}\right) = S(E,s)$$

physics interlude

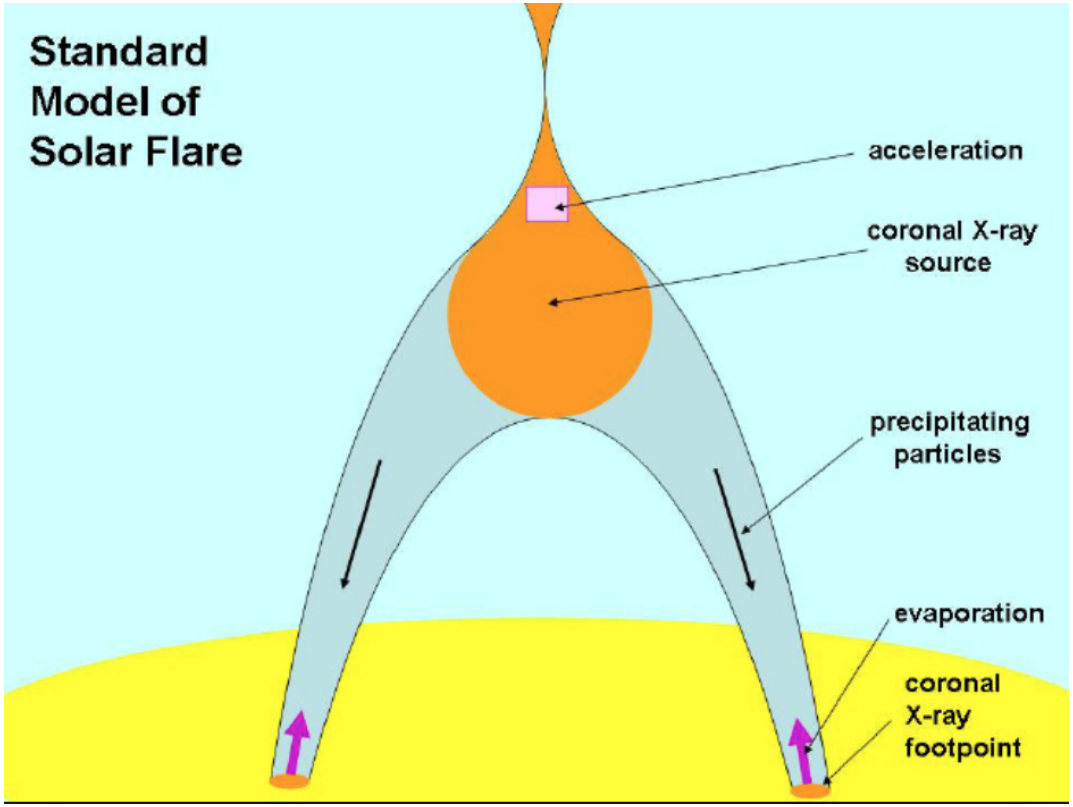

$$\frac{\partial F(E;s)}{\partial s} + \frac{\partial}{\partial E}\left(F(E,s)\frac{dE}{ds}\right) = S(E,s)$$

physics is in the electrons and its most direct signature is in (hard) X-rays

visibilities

data: reuven ramaty high energy solar spectroscopic imager (RHESSI)

visibilities

data: reuven ramaty high energy solar spectroscopic imager (RHESSI)

it is difficult to focus hard X-rays

visibilities

data: reuven ramaty high energy solar spectroscopic imager (RHESSI)

it is difficult to focus hard X-rays

it is easier to modulate them

visibilities

data: reuven ramaty high energy solar spectroscopic imager (RHESSI)

it is difficult to focus hard X-rays

it is easier to modulate them

rotating modulation collimators sample fourier components of the radiation flux
named visibilities

$$V(u_j, v_j; \epsilon) = \int\int f(x, y; \epsilon) e^{2\pi i(xu_j + yv_j)} dxdy \quad j = 1, \ldots, N$$

visibilities

data: reuven ramaty high energy solar spectroscopic imager (RHESSI)

it is difficult to focus hard X-rays

it is easier to modulate them

rotating modulation collimators sample fourier components of the radiation flux named visibilities

$$V(u_j, v_j; \epsilon) = \int \int f(x, y; \epsilon) e^{2\pi i(xu_j + yv_j)} dxdy \quad j = 1, \ldots, N$$

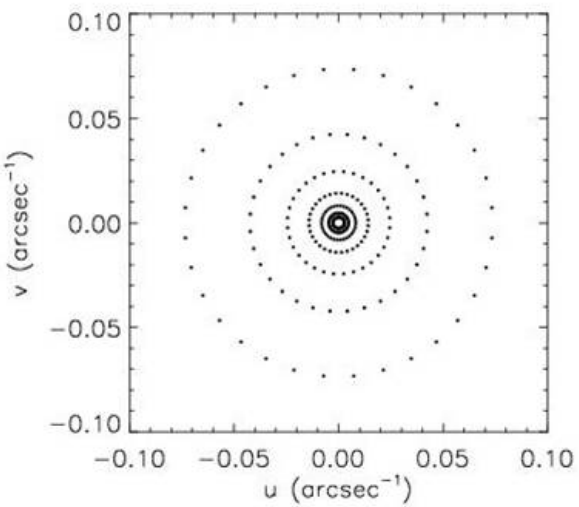

visibilities

data: reuven ramaty high energy solar spectroscopic imager (RHESSI)

it is difficult to focus hard X-rays

it is easier to modulate them

rotating modulation collimators sample fourier components of the radiation flux
named visibilities

$$V(u_j, v_j; \epsilon) = \int \int f(x, y; \epsilon) e^{2\pi i(xu_j + yv_j)} dxdy \quad j = 1, \ldots, N$$

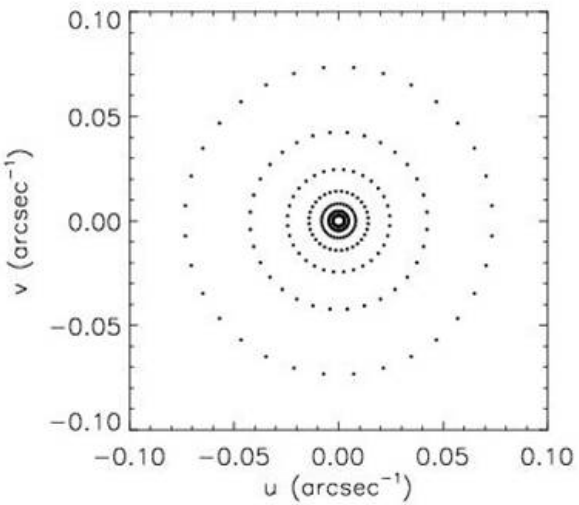

the image reconstruction problem is a
fourier inversion problem with limited data

visibilities

data: reuven ramaty high energy solar spectroscopic imager (RHESSI)

it is difficult to focus hard X-rays

it is easier to modulate them

rotating modulation collimators sample fourier components of the radiation flux
named visibilities

$$V(u_j, v_j; \epsilon) = \int \int f(x, y; \epsilon) e^{2\pi i (x u_j + y v_j)} dx dy \quad j = 1, \ldots, N$$

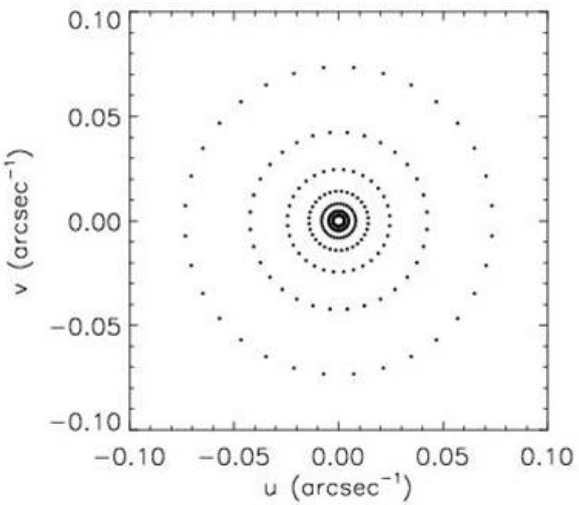

the image reconstruction problem is a fourier inversion problem with limited data

compressed sensing is the way

compressed sensing

in order for compressed sensing to work you need

- a sparse representation of the solution of the image reconstruction problem. this can be done by either
  - chasing for sparsity with respect to a catalogue of pre-defined image shapes (felix et al, *astrophys. j.*, 2017)

  or
  - chasing for sparsity with respect to a wavelet representation of the solution
- incoherence between the sampling domain and the sparsity-promoting domain. note that
  - the fourier domain in incoherent with respect to both the space and wavelet domains

finite isotropic wavelet transform

given $\psi_M(x)$ the 1D meyer mother function, the finite isotropic wavelet transform of $f \in L^2(\mathbb{R}^2)$ is

$$\hat{\psi}_{a,\mathbf{t}}(u,v) = a^{1/2}\hat{\psi}_M\left(a\sqrt{u^2+v^2}e^{-2\pi i(u,v)\cdot\mathbf{t}}\right)$$

given $\phi_M(x)$ the 1D meyer scaling function, the whole (u,v) is spanned by adding

$$\hat{\phi}(u,v) = \hat{\phi}_M(\sqrt{u^2+v^2})$$

finite isotropic wavelet transform

given $\psi_M(x)$ the 1D meyer mother function, the finite isotropic wavelet transform of $f \in L^2(\mathbb{R}^2)$ is

$$\hat{\psi}_{a,\mathbf{t}}(u,v) = a^{1/2}\hat{\psi}_M\left(a\sqrt{u^2+v^2}e^{-2\pi i(u,v)\cdot\mathbf{t}}\right)$$

given $\phi_M(x)$ the 1D meyer scaling function, the whole (u,v) is spanned by adding

$$\hat{\phi}(u,v) = \hat{\phi}_M(\sqrt{u^2+v^2})$$

the finite isotropic wavelet transform of f is

$$\mathcal{W}(f)(a,\mathbf{t}) = a^{1/2}\mathcal{F}^{-1}\left(\hat{f}(u,v)\hat{\psi}_M(a\sqrt{u^2+v^2})\right)(\mathbf{t})$$

finite isotropic wavelet transform

given $\psi_M(x)$ the 1D meyer mother function, the finite isotropic wavelet transform of $f \in L^2(\mathbb{R}^2)$ is

$$\hat{\psi}_{a,\mathbf{t}}(u,v) = a^{1/2}\hat{\psi}_M\left(a\sqrt{u^2+v^2}e^{-2\pi i(u,v)\cdot\mathbf{t}}\right)$$

given $\phi_M(x)$ the 1D meyer scaling function, the whole (u,v) is spanned by adding

$$\hat{\phi}(u,v) = \hat{\phi}_M(\sqrt{u^2+v^2})$$

the finite isotropic wavelet transform of f is

$$\mathcal{W}(f)(a,\mathbf{t}) = a^{1/2}\mathcal{F}^{-1}\left(\hat{f}(u,v)\hat{\psi}_M(a\sqrt{u^2+v^2})\right)(\mathbf{t})$$

theorem (duval poo, massone and piana, IEEE SampTA, 2017): the discretization of the functions $\psi_{a,\mathbf{t}}(x,y)$ and $\phi(x,y)$ provides a parseval frame

finite isotropic wavelet transform

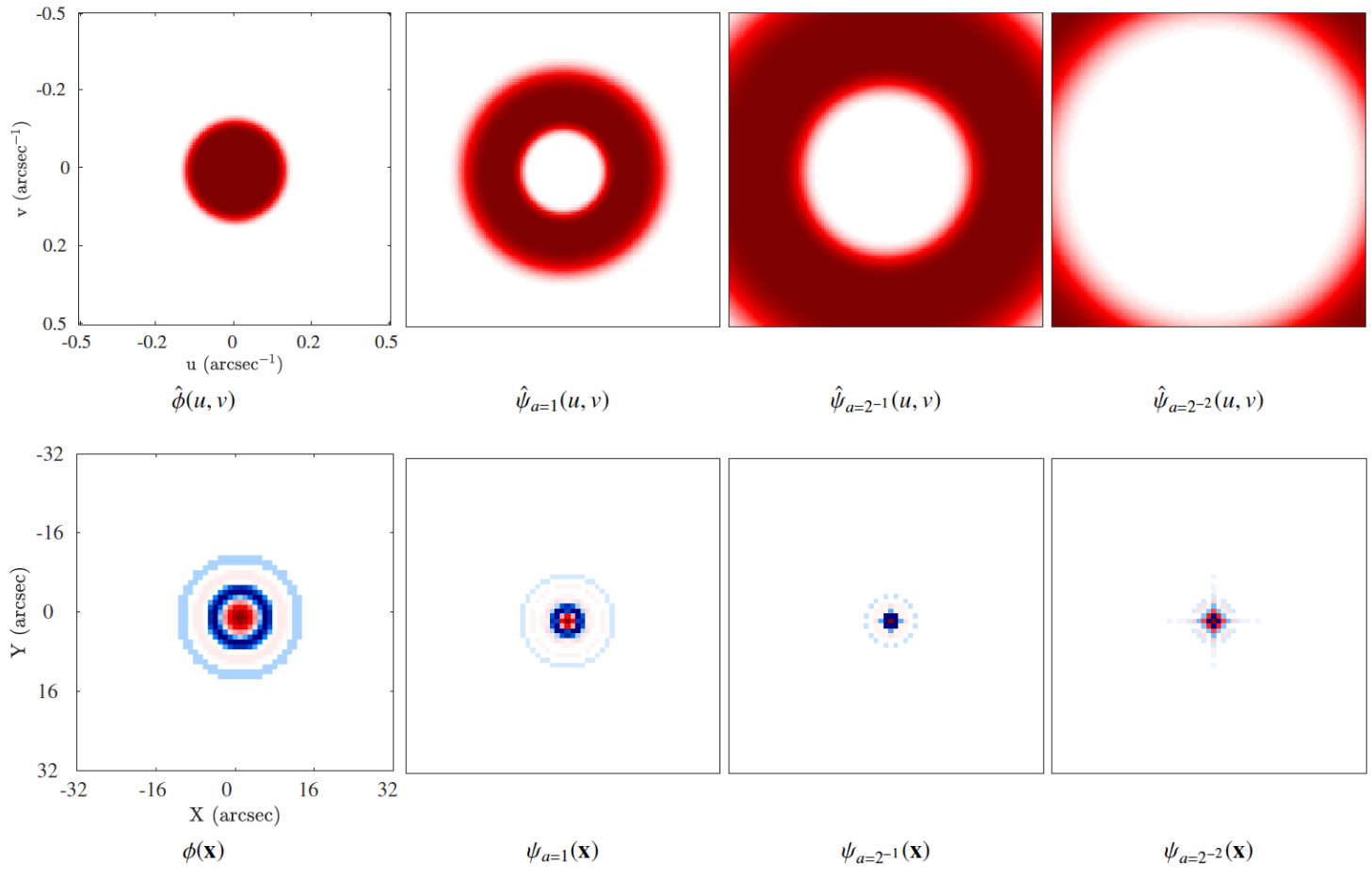

VIS_WV (duval poo, piana and massone, *astron. astrophys.*, in press)

given the image reconstruction problem

$$\mathbf{H} \cdot \mathcal{F}\mathbf{f} = \mathbf{V}$$

the VISibility-based finite isotropic WaVelet transform compressed sensing (VIS_WV) addresses the optimization problem

$$\min_{\mathbf{f}} \left\{ \|\mathbf{H} \cdot \mathcal{F}\mathbf{f} - \mathbf{v}\|_2^2 + \lambda \|\mathbf{W}\mathbf{f}\|_1 \right\} \tag{1}$$

VIS_WV (duval poo, piana and massone, *astron. astrophys.*, in press)

given the image reconstruction problem

$$\mathbf{H} \cdot \mathcal{F}\mathbf{f} = \mathbf{V}$$

the VISibility-based finite isotropic WaVelet transform compressed sensing (VIS_WV) addresses the optimization problem

$$\min_{\mathbf{f}} \left\{ \|\mathbf{H} \cdot \mathcal{F}\mathbf{f} - \mathbf{v}\|_2^2 + \lambda \|\mathbf{W}\mathbf{f}\|_1 \right\} \tag{1}$$

computational aspects:

- the minimum problem is solved by means of the fast iterative shrinkage-thesholding algorithm (FISTA) (beck and teboulle 2009)
- the reconstruction is robust with respect to the choice of the regularization parameter

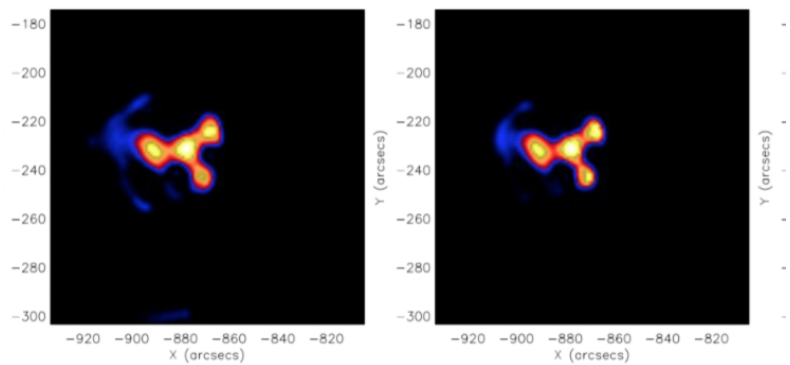

(b) $\lambda_L = 3.1 \times 10^{-3}$ (c) $\lambda_M = 5.7 \times 10^{-3}$

july 23 2002: reconstruction vs energy

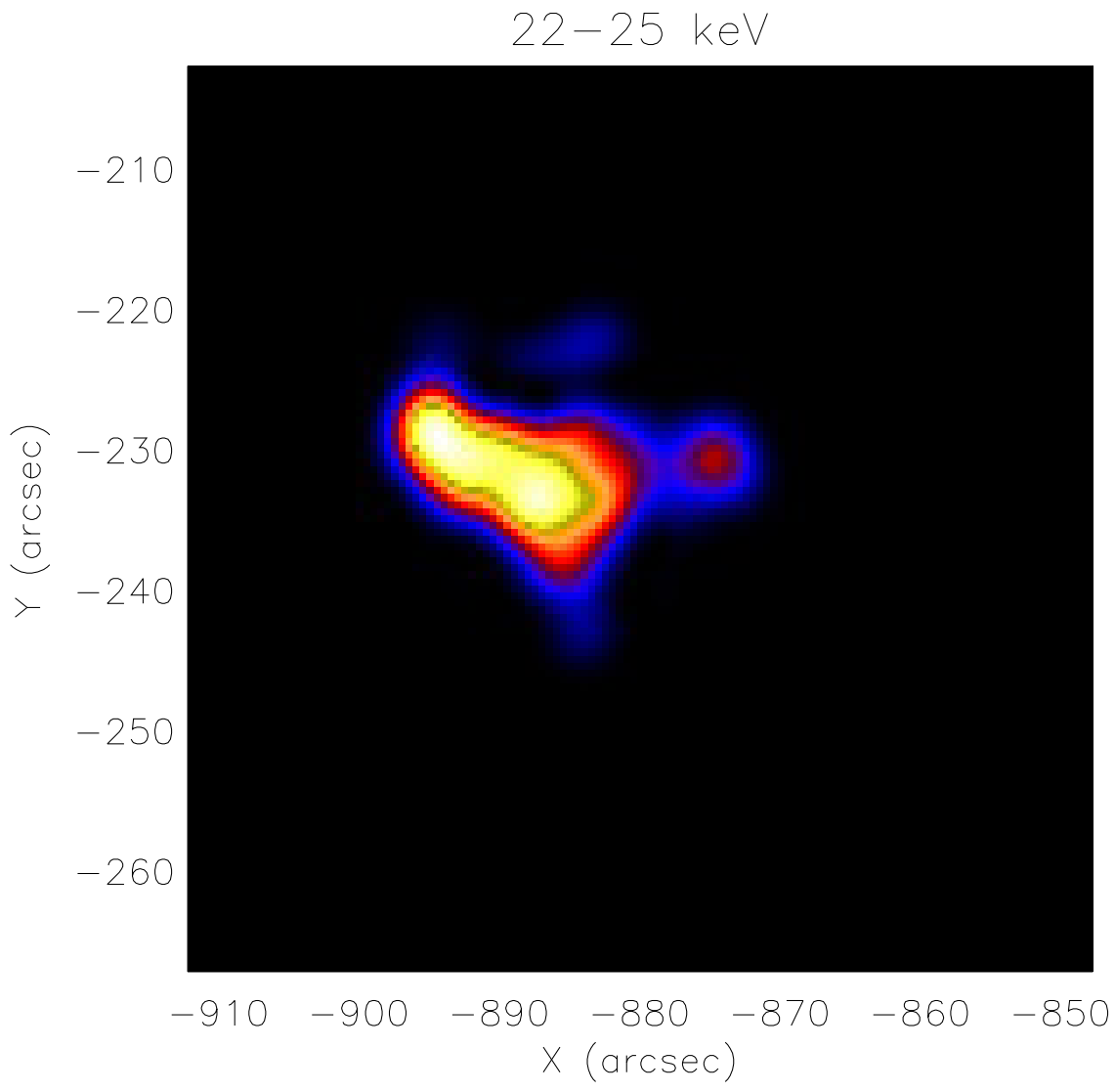

july 23 2002: reconstruction vs time

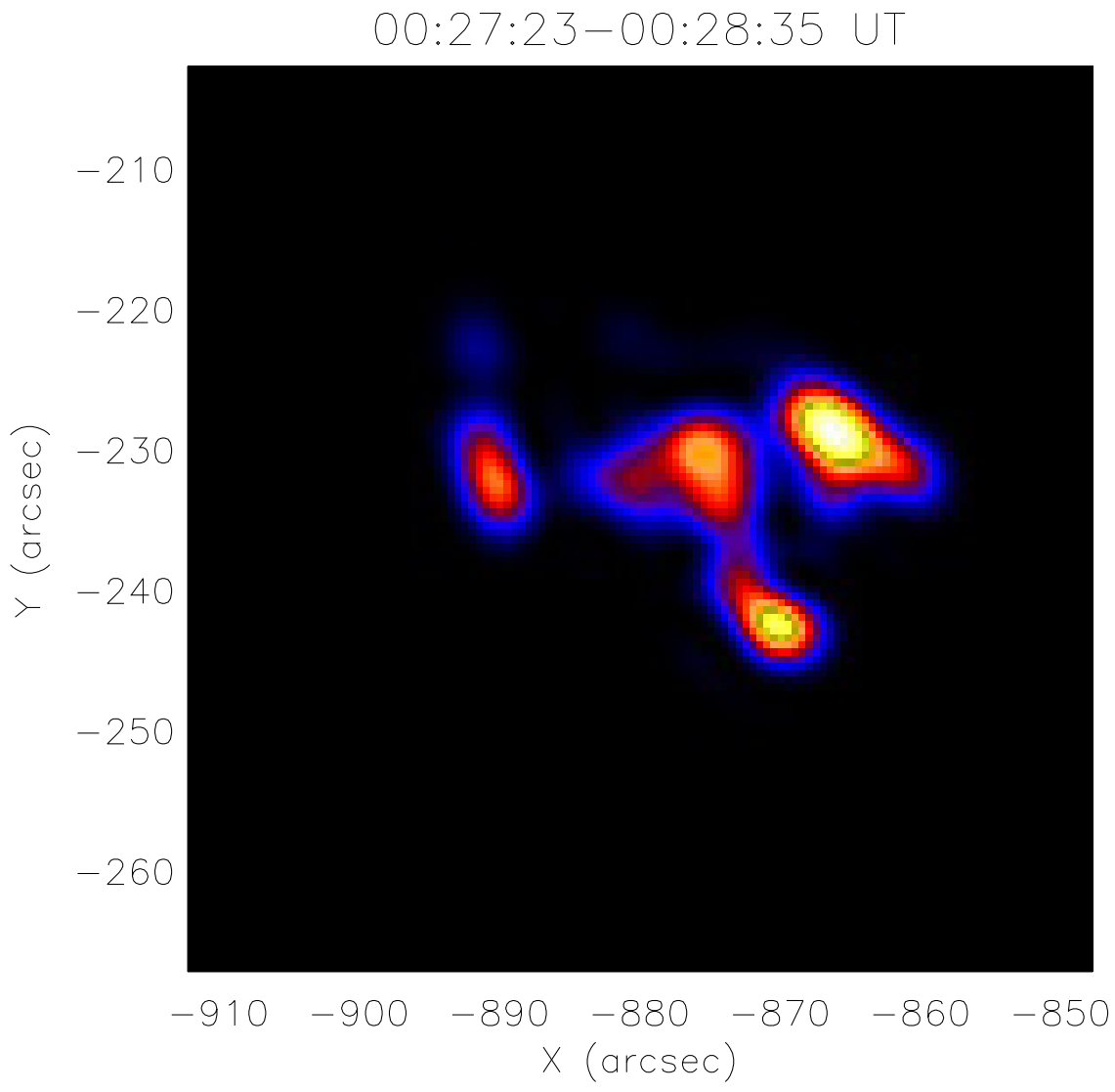

bremsstrahlung

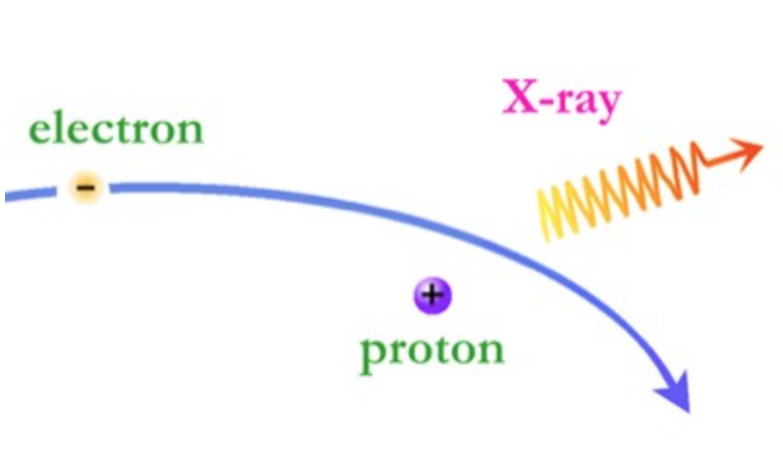

E: electron energy
ϵ: photon (X-ray) energy
$Q(\epsilon, E)$: bremsstrahlung cross-section
$g(\epsilon; x, y)$: X-ray spectrum at point (x, y) (i.e., grey level of pixel (x, y) in the reconstructed X-ray image at all energies ϵ)
$F(E; (x, y))$: electron spectrum at corresponding point (x, y) on the sun

$$g(\epsilon; x, y) = \int_0^\infty Q(\epsilon, E) F(E; x, y) dE$$

commuting operators

$$A : L^1(\mathbb{R}^2, L^2(0,\infty)) \to L^1(\mathbb{R}^2, L^2(0,\infty)) \quad AF : (x,y) \to \int_0^\infty Q(\cdot, E)F(E; x, y)dE$$

$$\hat{A} : L^1(\mathbb{R}^2, L^2(0,\infty)) \to L^1(\mathbb{R}^2, L^2(0,\infty)) \quad \hat{A}F : (u,v) \to \int_0^\infty Q(\cdot, E)F(E; u, v)dE$$

$$\mathcal{F} : L^1(\mathbb{R}^2, L^2(0,\infty)) \to L^1(\mathbb{R}^2, L^2(0,\infty)) \quad \mathcal{F}F : (u,v) \to \int_{\mathbb{R}^2} F(\cdot; x, y)e^{2\pi i(ux+vy)}dxdy$$

theorem (prato, p, emslie, hurford, kontar and massone, SIAM *j. imag. sci.*, 2009):

$$\mathcal{F}A = \hat{A}\mathcal{F}$$

commuting operators

$$A : L^1(\mathbb{R}^2, L^2(0,\infty)) \to L^1(\mathbb{R}^2, L^2(0,\infty)) \quad AF : (x,y) \to \int_0^\infty Q(\cdot, E)F(E;x,y)dE$$

$$\hat{A} : L^1(\mathbb{R}^2, L^2(0,\infty)) \to L^1(\mathbb{R}^2, L^2(0,\infty)) \quad \hat{A}F : (u,v) \to \int_0^\infty Q(\cdot, E)F(E;u,v)dE$$

$$\mathcal{F} : L^1(\mathbb{R}^2, L^2(0,\infty)) \to L^1(\mathbb{R}^2, L^2(0,\infty)) \quad \mathcal{F}F : (u,v) \to \int_{\mathbb{R}^2} F(\cdot;x,y)e^{2\pi i(ux+vy)}dxdy$$

theorem (prato, p, emslie, hurford, kontar and massone, SIAM *j. imag. sci.*, 2009):

$$\mathcal{F}A = \hat{A}\mathcal{F}$$

therefore, if

$$W(u,v;E) := \int_{\mathbb{R}^2} F(E;x,y)e^{-2\pi i(ux+vy)}dxdy$$

defines the (virtual) electron visibilities, then

$$V(u,v;\epsilon) = \int_0^\infty Q(\epsilon, E)W(u,v;E)dE$$

electron maps

$$V(u, v; \epsilon) = \int_0^\infty Q(\epsilon, E) W(u, v; E) dE$$

algorithm:

electron maps

$$V(u, v; \epsilon) = \int_0^\infty Q(\epsilon, E) W(u, v; E) dE$$

algorithm:

1. for each (u, v) in the frequency (experimental) domain, regularized spectral inversion provides an electron visibility spectrum

electron maps

$$V(u, v; \epsilon) = \int_0^\infty Q(\epsilon, E) W(u, v; E) dE$$

algorithm:

1. for each (u, v) in the frequency (experimental) domain, regularized spectral inversion provides an electron visibility spectrum
2. for each electron energy E, re-ordering and compressed sensing provides an electron maps

electron maps

$$V(u, v; \epsilon) = \int_0^\infty Q(\epsilon, E) W(u, v; E) dE$$

algorithm:

1. for each (u, v) in the frequency (experimental) domain, regularized spectral inversion provides an electron visibility spectrum
2. for each electron energy E, re-ordering and compressed sensing provides an electron maps

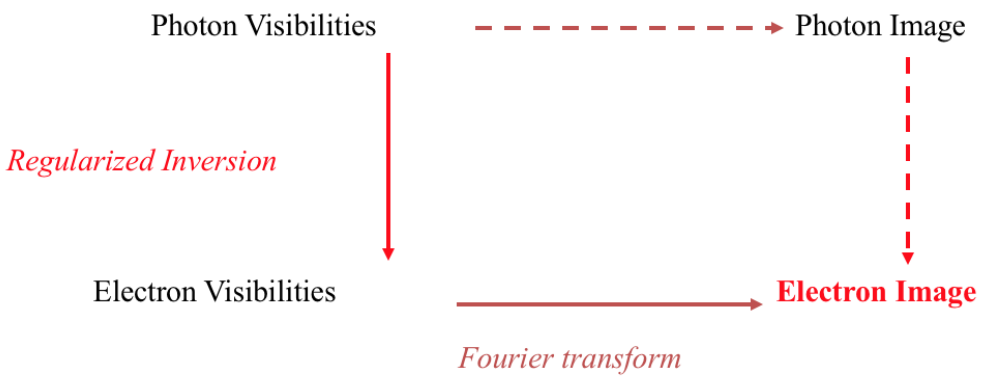

february 20 2002 event: photon maps

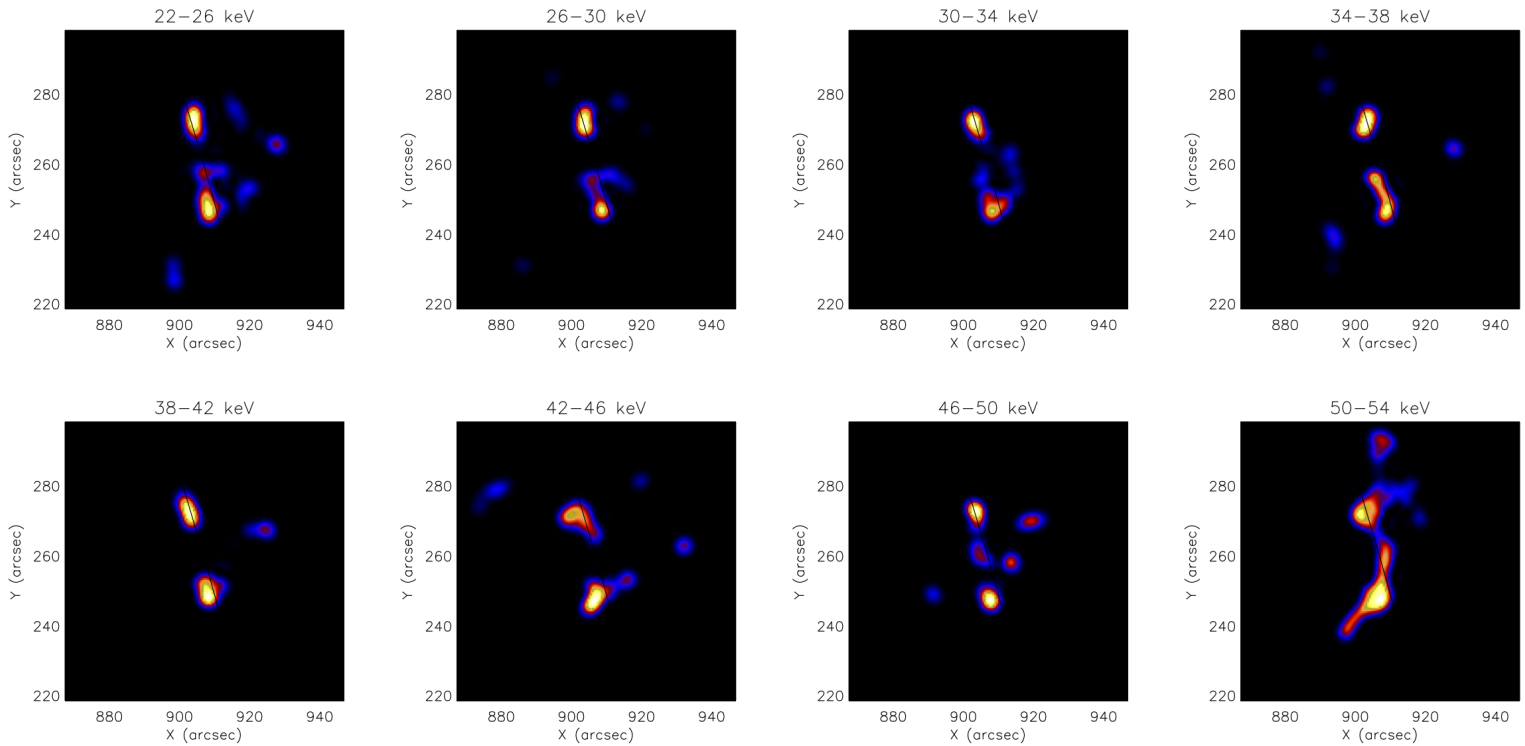

february 20 2002 event: electron maps

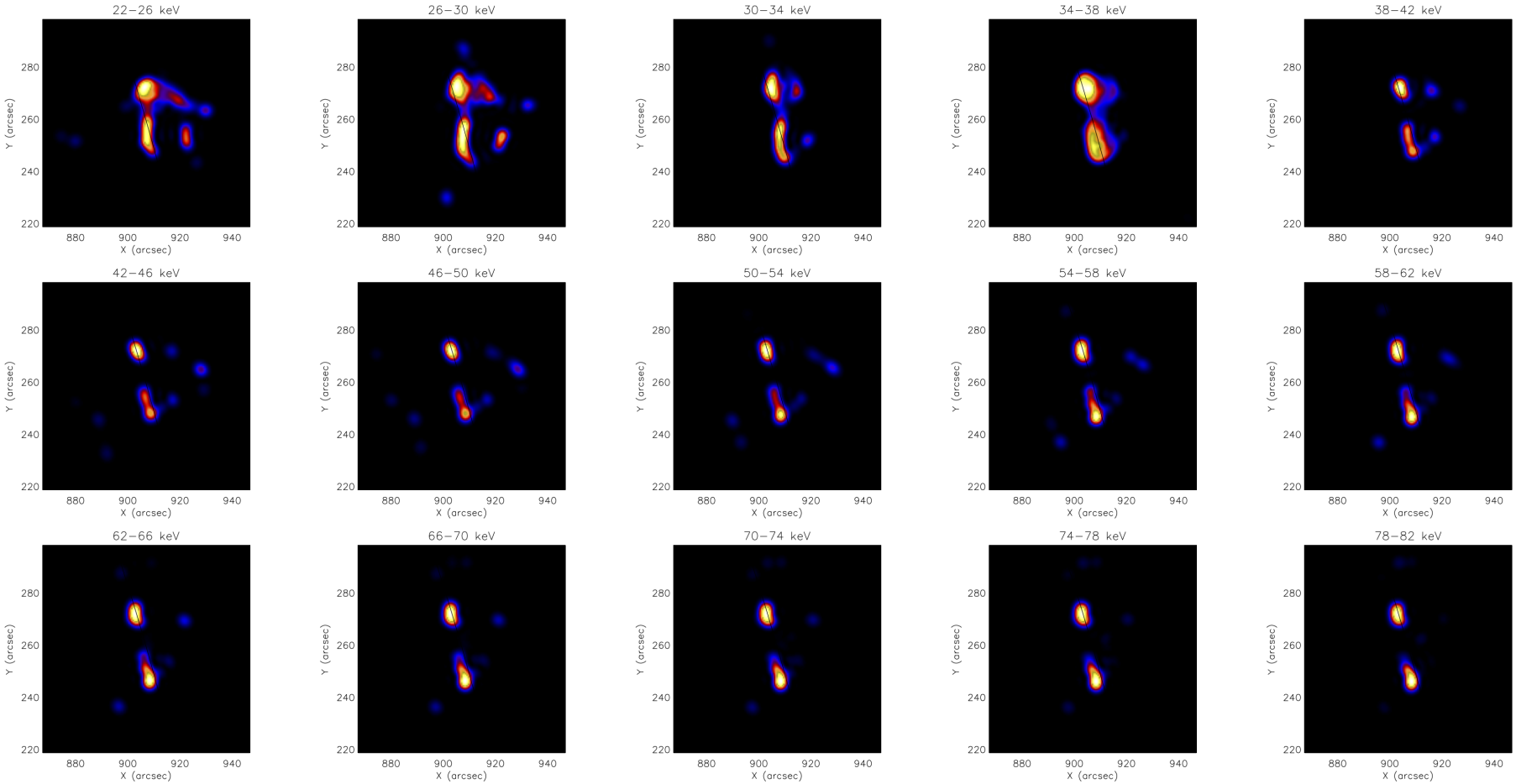

model calibration

$$\frac{\partial F(E;s)}{\partial s} + \frac{\partial}{\partial E}\left(F(E,s)\frac{dE}{ds}\right) = S(E,s)$$

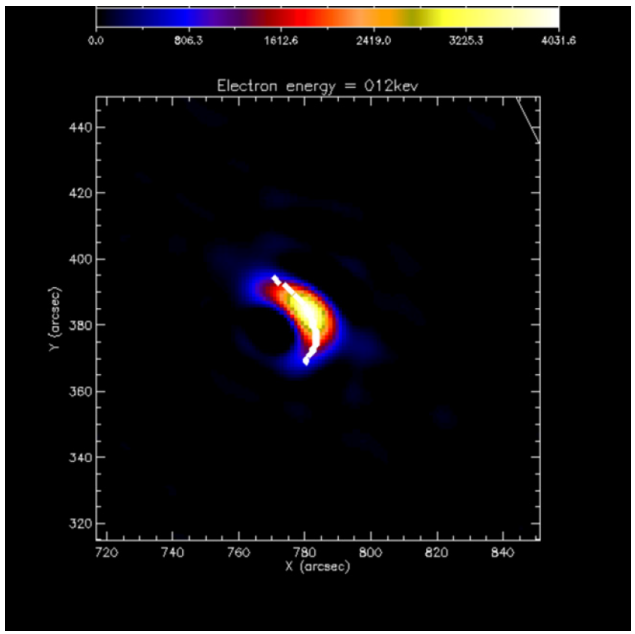

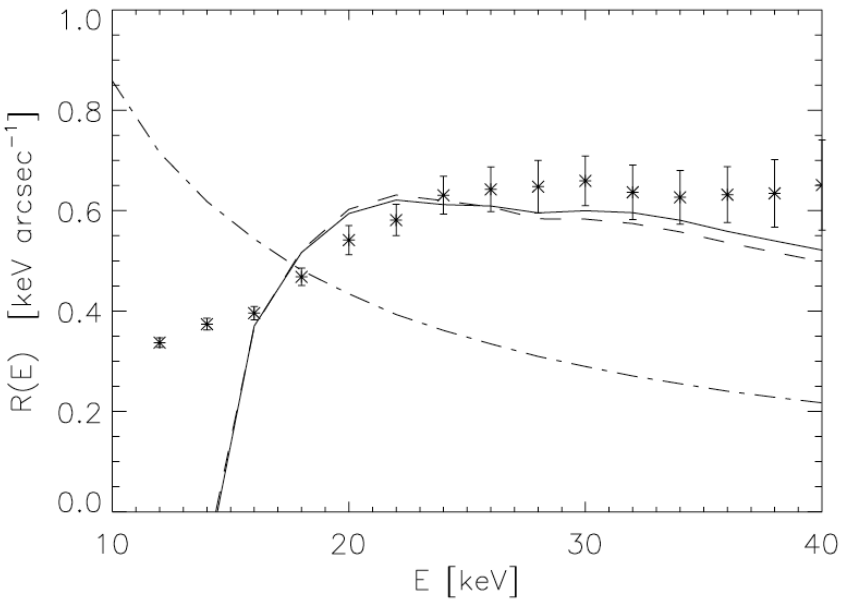

in progress - flare prediction

use space data in order to

- characterize the physical properties of the predicted flare
- determine which extracted features most impact the prediction effectiveness

	at least C1 flares						
	Hybrid Lasso	Hybrid Logit	SVC	Random Forest		average	std
flare_index_past	13,98	28,84	19,91	3,51		16,56	10,63
sharp_kw/hgradbh/total	3,47	37	18,59	16,57		18,95	13,87
wlsg_br/value_int	3,74	14,43	22,86	43,14		21,04	16,68
sharp_kw/jz/max	26,05	28	16,94	18,58		22,27	5,29
sharp_kw/usiz/max	24,2	36,75	34,79	18,37		28,53	8,73
wlsg_blos/value_int	3,96	45	46,61	25,39		30,24	20,00
r_value_br_logr	3,52	2,81	128,91	7,47		35,68	62,19
sharp_kw/ggt45fract	14,99	32	57,6	49,3		38,35	19,00
sharp_kw/usiz/stddev	17,15	49,46	54,26	45,89		41,69	16,72
sharp_kw/gamma/total	61,65	20,76	52,95	34,67		42,51	18,35

in progress - image reconstruction

new telescopes upcoming:

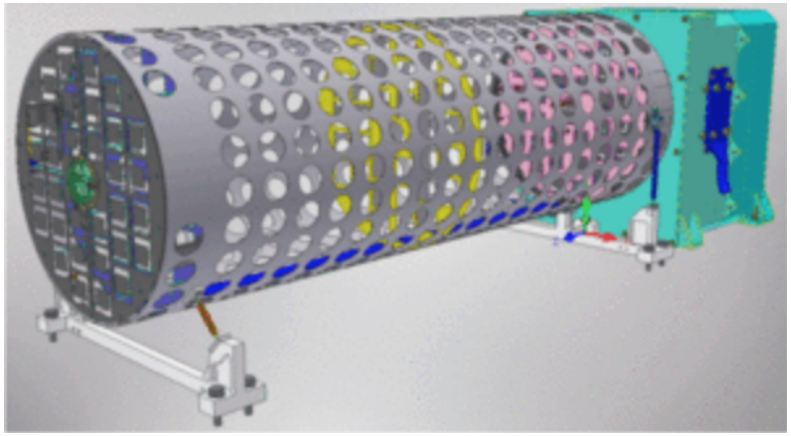

- ESA
- launch: 2019 or 2020
- visibilities
- fourier-based methods

- NASA
- phase b
- focused-based optics
- fredholm integral equation

credits

thanks to:

credits

thanks to:

- anna maria massone (UNIGE and CNR): hard X-ray spectroscopy, imaging, imaging spectroscopy; de-saturation of EUV images; flare prediction; co-I for STIX and FOXSI

credits

thanks to:

- anna maria massone (UNIGE and CNR): hard X-ray spectroscopy, imaging, imaging spectroscopy; de-saturation of EUV images; flare prediction; co-I for STIX and FOXSI
- federico benvenuto (UNIGE): hard X-ray imaging; de-saturation of EUV images; flare prediction

credits

thanks to:

- anna maria massone (UNIGE and CNR): hard X-ray spectroscopy, imaging, imaging spectroscopy; de-saturation of EUV images; flare prediction; co-I for STIX and FOXSI
- federico benvenuto (UNIGE): hard X-ray imaging; de-saturation of EUV images; flare prediction
- cristina campi (UNIPD): flare prediction

credits

thanks to:

- anna maria massone (UNIGE and CNR): hard X-ray spectroscopy, imaging, imaging spectroscopy; de-saturation of EUV images; flare prediction; co-I for STIX and FOXSI
- federico benvenuto (UNIGE): hard X-ray imaging; de-saturation of EUV images; flare prediction
- cristina campi (UNIPD): flare prediction
- alberto sorrentino, miguel duval-poo, federica sciacchitano (UNIGE): hard X-ray imaging

credits

thanks to:

- anna maria massone (UNIGE and CNR): hard X-ray spectroscopy, imaging, imaging spectroscopy; de-saturation of EUV images; flare prediction; co-I for STIX and FOXSI
- federico benvenuto (UNIGE): hard X-ray imaging; de-saturation of EUV images; flare prediction
- cristina campi (UNIPD): flare prediction
- alberto sorrentino, miguel duval-poo, federica sciacchitano (UNIGE): hard X-ray imaging
- sabrina guastavino (UNIGE): flare prediction; de-saturation of EUV images

credits

thanks to:

- anna maria massone (UNIGE and CNR): hard X-ray spectroscopy, imaging, imaging spectroscopy; de-saturation of EUV images; flare prediction; co-I for STIX and FOXSI
- federico benvenuto (UNIGE): hard X-ray imaging; de-saturation of EUV images; flare prediction
- cristina campi (UNIPD): flare prediction
- alberto sorrentino, miguel duval-poo, federica sciacchitano (UNIGE): hard X-ray imaging
- sabrina guastavino (UNIGE): flare prediction; de-saturation of EUV images

credits

thanks to:

- anna maria massone (UNIGE and CNR): hard X-ray spectroscopy, imaging, imaging spectroscopy; de-saturation of EUV images; flare prediction; co-I for STIX and FOXSI
- federico benvenuto (UNIGE): hard X-ray imaging; de-saturation of EUV images; flare prediction
- cristina campi (UNIPD): flare prediction
- alberto sorrentino, miguel duval-poo, federica sciacchitano (UNIGE): hard X-ray imaging
- sabrina guastavino (UNIGE): flare prediction; de-saturation of EUV images

credits

thanks to:

- anna maria massone (UNIGE and CNR): hard X-ray spectroscopy, imaging, imaging spectroscopy; de-saturation of EUV images; flare prediction; co-I for STIX and FOXSI
- federico benvenuto (UNIGE): hard X-ray imaging; de-saturation of EUV images; flare prediction
- cristina campi (UNIPD): flare prediction
- alberto sorrentino, miguel duval-poo, federica sciacchitano (UNIGE): hard X-ray imaging
- sabrina guastavino (UNIGE): flare prediction; de-saturation of EUV images

credits

thanks to:

- anna maria massone (UNIGE and CNR): hard X-ray spectroscopy, imaging, imaging spectroscopy; de-saturation of EUV images; flare prediction; co-I for STIX and FOXSI
- federico benvenuto (UNIGE): hard X-ray imaging; de-saturation of EUV images; flare prediction
- cristina campi (UNIPD): flare prediction
- alberto sorrentino, miguel duval-poo, federica sciacchitano (UNIGE): hard X-ray imaging
- sabrina guastavino (UNIGE): flare prediction; de-saturation of EUV images